Retrieval of spectral aerosol optical thickness over land using ocean color sensors MERIS and SeaWiFS

W. von Hoyningen-Huene, J. Yoon, M. Vountas, L. G. Istomina, G. Rohen, T. Dinter, A. A. Kokhanovsky, and J. P. Burrows

Institute of Environmental Physics, University of Bremen, Bremen, Germany

Correspondence to: W. von Hoyningen-Huene (hoyning@iup.physik.uni-bremen.de)

1

Abstract

abstr For the determination of aerosol optical thickness (AOT) Bremen AErosol Retrieval (BAER) has been developed. Method and main influences on the aerosol retrieval are described together with validation and results. The retrieval separates the spectral aerosol reflectance from surface and Rayleigh path reflectance for the shortwave range of the measured spectrum of top-of-atmosphere reflectance less than $0.670\,\mu m$. The advantage of MERIS (Medium Resolution Imaging Spectrometer on the Envirinmental Satellite - ENVISAT - of the European Space Agency - ESA) and SeaWiFS (Sea viewing Wide Field Sensor on OrbView-2 space craft) observations are the existence of several spectral channels in the blue and visible range enabling the spectral determination of AOT in 7 (or 6) channels (0.412–$0.670\,\mu m$) and additionally channels in the NIR, which can be used to characterize the surface properties. A dynamical spectral surface reflectance model for different surface types is used to obtain the spectral surface reflectance for this separation. Normalized differential vegetation index (NDVI), taken from the satellite observations, is the model input. Further surface bi-directional reflectance distribution function (BRDF) is considered by the Raman-Pinty-Verstraete (RPV) model. Spectral AOT is obtained from aerosol reflectance using look-up-tables, obtained from radiative transfer calculations with given aerosol phase functions and single scattering albedos either from aerosol models, given by model package 'optical properties of aerosol components' (OPAC) or from experimental campaigns. Validations of the obtained AOT retrieval results with data of Aerosol Robotic Network (AERONET) over Europe gave a preference for experimental phase functions derived from almucantar measurements. Finally long-term observations of SeaWiFS have been investigated for 11 year trends in AOT. Western European regions have negative trends with decreasing AOT with time. For the investigated Asian region increasing AOT have been found.

1 Introduction

introSeveral applications in climate research and environmental control require a determination of spectral aerosol optical thickness. Since most of the aerosol source regions are on land,

2

retrieval methods for applications over land are of importance. Other than over ocean, where the surface reflectance in the NIR is negligible and the retrieval approaches can assume as "black" surface, land surface cannot be assumed as "black" and need to be estimated and corrected. Therefore all land applications for the determination of aerosol need a separation of land surface properties from atmosphere before one can retrieve aerosol optical thickness.

Dual- or multi-view techniques, like in approaches using data of the ATSR-2, AATSR ((Advanced) Along Track Scanning Radiometer) or the MISR (Multiangle Imaging SpectroRadiometer) instruments, can separate the surface properties from two collocated observations under different viewing angles, assuming atmosphere and surface can be described sufficiently for both observations.

Ocean colour sensors, like MERIS or SeaWiFS are single view instruments and the spectral surface contribution needs to be estimated from the observed spectral properties of top-of-atmosphere reflectance. Retrieval approaches for such sensors are provided by von Hoyningen-Huene et al., 2003 and Hsu et al., 2004. An overview of the present status of aerosol retrieval from space is given in several contributions to Kokhanovsky and de Leeuw, 2009. The aim of this contribution is to describe the aerosol remote sensing approach Bremen AErosol Retrieval (BAER) for multi-spectral single-view instruments in its present status. Since from its first publication (von Hoyningen-Huene et al., 2003) several improvements have been made, which will be presented here. The main change compared to older publications is the consideration of a non-Lambertian surface, which reduced the random sacttering of the retrieved AOT results in comparison with ground-based observations as shown in Dinter et al., 2009.

2 Requirements for ocean colour instruments for aerosol investigations over land

Since the surface contribution cannot be neglected in an aerosol retrieval over land, like over ocean, it needs to be corrected. Therefore a retrieval of aerosol optical thickness (AOT) over land requires sufficient spectral information on top-of-atmosphere (TOA) reflectance in the blue, VIS and NIR channels, to estimate the surface contribution, its spectral properties and to correct

3

them for suitable channels, where the surface contribution is weak. One needs a spectral region, where the surface reflectance is low enough to be corrected and to perform the aerosol retrieval. Furthermore a spectral region is needed, where information on the surface properties, like the vegetation status can be estimated.

Figure 1 illustrates the general different properties of the TOA reflectance and its components over land (left) and ocean (right).

Over ocean the surface reflectance as well the Rayleigh path reflectance is low in the NIR for wavelength $\lambda > 0.67\,\mu m$. Thus aerosol is the dominating influence. Therefore over ocean conditions this region is used for the retrieval of the spectral AOT.

Over land the NIR is dominated by the highly variable strong reflectance of the land surface, as there is the high reflectance of the green vegetation, changing with vegetation type, status and vegetation cover. Generally, land surface reflectance decreases with decreasing wavelength. Since for the aerosol retrieval the surface reflectance in the blue and UV part of the spectrum cannot be neglected, it needs to be estimated in an adequate way. Although Rayleigh path reflectance increases with decreasing wavelength, it can be calculated with sufficient accuracy, because wavelength and air pressure are known.

Thus, instruments for the retrieval of AOT over land require channels in the blue and short-wave visible spectral region for the retrieval of the aerosol and additionally channels in the NIR to estimate the surface properties. The spectral channels of the MERIS and SeaWiFS instruments are listed in Table 1. In Table 1 the channels used for the aerosol retrieval over land are indicated by AOT(L) and the channels used for the estimation of surface properties by NDVI (Normalized Differential Vegetation Index). Channels, used for AOT retrieval over ocean are indicated by AOT(O).

If the requirements of the WMO Global Climate Observing System (GCOS, 2006) should be fulfilled, AOT should be determined with 0.01. For a resolution of AOT of $\pm\,0.01$, depending on the aerosol type, the aerosol reflectance should be detected within $\pm\,0.001$. If all other influences were known, then this is the required accuracy of TOA reflectance. Therefore for the task of aerosol retrieval instruments with large signal-to-noise-ratio - SNR ($\geq$1000) should be preferred, like MERIS, SeaWiFS or MODIS. Unless this requirement, the needed assumptions,

4

used by satellite based aerosol retrievals in general will presently not satisfy this requirement.

The absolute accuracy in TOA reflectance is for MERIS about 3% (Delwart et al., 2003, Martiny et al., 2005a) and SeaWiFS 4% (Martiny et al., 2005b). This is sufficient, if one considers that disturbing effects, like land surface and Rayleigh path reflectance, are not accounted in the above estimation. For the aerosol retrieval over land it is of importance, that the instrument does not reach saturation in its radiometric sensitivity. There is no saturation problem in the cases of MERIS and SeaWiFS. Unfortunately the ocean channels of the Moderate Resolution Imaging Spetroradiometer (MODIS), which have the same wavelengths as SeaWiFS saturate under some land conditions. Thus MODIS land and atmospheric channels have to be used with deviating wavelengths from MERIS and SeaWiFS BAER variants.

The maximal spatial resolution of MERIS is 0.3×0.3 km in the full resolution mode (FR). However for the retrieval of AOT mostly the reduced resolution mode (RR) is used with 1.1×1.1 km. This is similar to the local area cover (LAC) of the SeaWiFS instrument with 1.1×1.1 km or to 1×1 km agglomerated data of the MODIS instrument. SeaWiFS data are provided also in global area cover (GAC) with about 4.5×4.5 km.

A summary and comparison of the instrument parameters, like swath width, spatial resolution, coverage and repetition time is given in Table 2.

The SeaWiFS instrument has the advantage over MERIS and MODIS to operate in a mode 20 deg tilted away from the sun in the direction of the track. This avoids strong sun-glint effects over the ocean. It also reduces the BRDF effects from land surface, that the BRDF model in Sect. 3.3 is not so sensitive to the parameter choice. Since for MERIS no techniques are applied to avoid sun-glint, over ocean about 40% of the swath is contaminated by sun-glint in lower latitudes.

5

3   Bremen AErosol Retrieval (BAER)

3.1   Main steps of BAER

The main steps of BAER described in detail in the following sections are summarized in Figure 2.

The reading procedure selects the needed measured and auxiliary data for the determination of the required aerosol reflectance. These are solar and viewing geometry, geographical coordinates, TOA radiance, extraterrestrial solar radiation and prepares the TOA reflectance for the retrieval of aerosol reflectance and AOT. Also the surface elevation data for the consideration in the Rayleigh path reflectance are taken from a digital elevation model, GTOPO30 from US Geological Survey (USGS) and will be assimilated with the scene.

At first a discrimination step analyses the TOA reflectance ρ_{TOA} (0.865 μm) at the wavelength of 0.865 μm and the surface elevation data z to discriminate land, ocean and clouds and directs the scene to the corresponding routines of the program. Land is selected if z > 0 m and $\rho_{TOA} \geq 0.1$, ocean is selected with z = 0 m and $\rho_{TOA} < 0.1$ and clouds are selected by the cloud screening of Sect. 3.6. Additionally the NDVI (Normalized Differential Vegetation Index), Eq. (6) is used to discriminate land from water.

For ocean targets the an ocean surface is used instead of the land surface and the ocean algorithm is therefore much more simple than the land part. It can benefit of the low water surface reflectance in the NIR channels of the instruments and use therefore all MERIS or SeaWiFS channels. The principle of the ocean algorithm is the same as for the land algorithm with different surface properties. Thus we do not describe the ocean algorithm separately.

Aerosol reflectance as it is described in 3.3. will be determined for cloud free land and ocean targets, and if it is obtained, AOT according section 3.4 is retrieved. For this Rayleigh path reflectance is calculated for the given illumination and viewing geometry conditions, the height conditions, using barometric pressure equation and dry adiabatic lapse rate for the consideration of elevation effects for the determination of Rayleigh optical thickness and air mass factors.

After this step the surface reflectance model (Eq. 6) is used for the initialization of the iterative determination of spectral AOT: (a) determination of aerosol reflectance, (b) derivation of

6

AOT by the selected LUT, (c) analysis of the smoothness of spectral AOT by RMSD between retrieved and Angström power law approximation and (d) correction of spectral surface reflectance until RMSD < 0.005 or return to (a). The iterative procedure to constrain smoothness is described in section 3.5.

If the RMSD has reached 0.005, then the spectral AOT for all channels below the red edge is obtained. Together with this the Angström spectral slope α for the spectral range of 0.412–0.865 μm is found. With this an extrapolation of spectral AOT for all MERIS channels above the red edge is made and an atmospheric correction is performed to calculate spectral surface reflectance for all MERIS channels.

3.2 The TOA reflectance

Nadir viewing satellite instruments generally measure the up-welling directed radiance $L^{\uparrow}$, giving the top of atmosphere (TOA) reflectance $\rho_{\mathrm{TOA}}(\lambda) = \frac{\pi L^{\uparrow}(\lambda)}{E_0(\lambda)\cdot\cos(z_0)}$, by reference to its solar irradiation E_0, for the zenith distance z_0 for each considered wavelength λ. The spectral dependence of all radiative properties is omitted in the following equations. Following Kaufman et al., 1997, the top-of-atmosphere reflectance (Eq. 1) is composed of the atmospheric path reflectance $\rho_{\mathrm{Atmos}}^{\mathrm{Black}}$ and the surface contribution, influenced by the atmosphere (second term). There $\rho_{\mathrm{Atmos}}^{\mathrm{Black}}$ is the atmospheric path reflectance for a "black" surface. It depends on δ_{Aer}, δ_{Ray}- the optical thickness for aerosol and Rayleigh scattering, $p(\theta)$ is the atmospheric phase function, composed of aerosol and Rayleigh scattering, depending on scattering angle θ, ω_0- the single scattering albedo of atmosphere and the geometry conditions, the zenith distances for illumination z_0 and viewing z_S and the relative azimuth ϕ. The second term is determined by the surface albedo A_{Surf}, the total transmission t_{tot} for the illumination and viewing geometry and the hemispheric reflectance r_{Hem}.

$$\rho_{\mathrm{TOA}}(z_0,z_S,\phi) = \rho_{\mathrm{Atmos}}^{\mathrm{Black}}(z_0,z_S,\phi,\delta_{\mathrm{Aer}},\delta_{\mathrm{Ray}},p(\theta),\omega_0,0) + \frac{t_{\mathrm{tot}}(z_0)t_{\mathrm{tot}}(z_S)A_{\mathrm{Surf}}(z_0,z_S)}{1-A_{\mathrm{Surf}}(z_0,z_S)r_{\mathrm{Hem}}(\delta_{\mathrm{tot}},g)} \quad (1)$$

Equation (1) is valid for each wavelength, e.g. all parameters have to be known with their spectral properties for the channels used.

7

This equation is in a good agreement with reality, if ocean conditions in the red and NIR are known.

However, over land with a real surface reflectance, which is not "black", multiple scattering between surface and atmosphere introduces coupling terms between all components of the radiation transfer, causing deviations from idealized assumptions. Further the combined atmospheric path reflectance disables a simple separation of the aerosol path reflectance for a retrieval of aerosol optical thickness from the combination with the Rayleigh scattering and multiple scattering effects.

3.3 Aerosol reflectance over land

The basic approach of the Bremen AErosol Retrieval (BAER) is described in von Hoyningen-Huene et al., 2003, 2006.

For the retrieval of aerosol optical thickness, the separation of aerosol reflectance from top-of-atmosphere reflectance is required by correcting for the Rayleigh path reflectance ρ_{Ray} and the surface term.

$$\rho_{\mathrm{Aer}}(z_0,z_S,\phi,\delta_{\mathrm{Aer}},p_{\mathrm{Aer}}(\theta),\omega_0,0) = \rho_{\mathrm{TOA}}(z_0,z_S,\phi) - \rho_{\mathrm{Ray}}(z_0,z_S,\phi,\delta_{\mathrm{Ray}},p,0) - \frac{t_{\mathrm{tot}}(z_0)t_{\mathrm{tot}}(z_S)A_{\mathrm{Surf}}}{1 - A_{\mathrm{Surf}}r_{\mathrm{hem}}(\delta_{\mathrm{tot}},g)} \quad (2)$$

Rayleigh path reflectance ρ_{Ray} is calculated by a radiative transfer model, using Rayleigh optical thickness for the given wavelength (Buchholz, 1995), the Rayleigh phase function, the illumination and viewing geometry and the actual temperature and pressure conditions at the surface. Barometric height equation and dry adiabatic lapse rate are used together with the digital elevation model (GTOPO30) to correct Rayleigh path reflectance and air mass factors to the actual conditions within the satellite scene, $\delta_{\mathrm{Ray}}(\lambda,p,T) = \frac{p}{p_0} \cdot \frac{T_0}{T} \cdot \delta_{\mathrm{Ray}}(\lambda)$. Sea level pressure p_0 is taken from ECMWF data or if not available as standard pressure, T_0 is obtained from a climatology of Max-Planck-Institute in Hamburg.

The correction of the surface effects requires the application of a surface model, which can be adapted to the spectral and geometry conditions of the satellite scene. The consideration of the surface term requires the knowledge of the spectral surface albedo A_{Surf}, if the surface can be assumed as Lambertian. Investigations of Dinter et al., 2009 showed significant bias in the

8

AOT depending on swath position, if Lambertian surface is used. Since the land surface is in reality a non-Lambertian ground, the spectral surface albedo has to be substituted by directed spectral surface reflectance:

$$\rho_{\text{Surf}}(\lambda, z_0, z_S, \phi) = \text{BRDF}(z_0, z_S, \phi) \cdot A(\lambda) \tag{3}$$

$\text{BRDF}(z_0, z_S, \phi)$ is the normalized bi-directional reflection function to the nadir position, based on the Raman-Pinty-Verstraete model (RPV), (Maignan et al, 2004) describing the relative deviation of the reflectance for the given illumination and viewing conditions. Examples are presented in Figure 3. The relative BRDF shows a significant deviation from Lambertian conditions ($\text{BRDF}(z_0, z_S, \phi)$=const =1.0). The shape of the BRDF can be described by 3 parameters. Since the parameters depend on surface type, the selection of the appropriate shape parameters is a still open task. The analysis of POLDER observations can help to establish a regional data base of the required parameters. Ignoring BRDF leads to a bias of AOT along the viewing geometry or requires apparent aerosol phase functions, including BRDF effects.

The present realization uses one set of BRDF parameters for the whole scene, ignoring regional variations. The BRDF parameters to be used are still under investigation, because it is variable and depending on surface type. The normalized BRDF is used as

$$\text{BRDF}(z_0, z_S, \phi, \lambda) = \frac{\text{BRDF}^*(z_0, z_S, \phi, \lambda)}{\text{BRDF}^*(z_0, z_S = 0, \phi, \lambda)}, \tag{4}$$

where BRDF* is described by the RPV model.

$$\text{BRDF}^*(z_0, z_S, \phi, \lambda) = \rho_{\text{Surf}}(\lambda) \cdot \frac{\cos^{k-1} z_0 \cdot \cos^{k-1} z_S}{(\cos z_0 + \cos z_S)^{1-k}} \cdot \frac{1 - \varphi^2}{(1 + \varphi^2 - 2\varphi \cos(\pi - \arccos\theta))^{1.5}} \cdot (1 + \frac{1 - \rho(\lambda)}{1 + G}) \tag{5}$$

with $G = \sqrt{\tan^2 z_0 + \tan^2 z_S - 2 \cdot \tan z_0 \cdot \tan z_S \cdot \cos\phi}$.

The input parameters are $\rho_{\text{Surf}}(\lambda)$, taken from a first guess with Eq. (6), made for Lambertian conditions (BRDF=1), and k and φ. k described the surface anisotropy and φ the forward − backward scattering of the surface. Thus the diffuse directed reflection of the surface can be described. As preliminary values, $k = 0.65$ and $\varphi = -0.06$ are used, obtained from sites over

9

Germany, minimizing the AOT deviations from ground based AERONET data. With these settings the bias along the viewing geometry of the Lambertian ground could be reduced for MERIS observations. However, not all regional variations disappear and a regional variable data set is required. For SeaWiFS data the sensor tilt reduces the BRDF effect, thus the values found over Germany seem to be sufficient.

The spectral properties and the magnitude of the surface are described by the spectral albedo, described by a linear mixing model, using two basic spectra for "green vegetation" $\rho_{\text{Veg}}(\lambda)$ and "bare soil" $\rho_{\text{Soil}}(\lambda)$. Since the spectral properties of the surface reflectance will be expressed by $\rho_{\text{Surf}}^{\diamond}(\lambda) = C_{\text{Veg}} \cdot \rho_{\text{Veg}}(\lambda) + (1 - C_{\text{Veg}}) \cdot \rho_{\text{Soil}}(\lambda)$, the surface albedo will be

$$A_{\text{Surf}}(\lambda, z_0, z_S, \phi) = \frac{\text{SF}}{\text{BRDF}(z_0, z_S, \phi)} \cdot \rho_{Surf}^{\diamond}$$
$$= \frac{\text{SF}}{\text{BRDF}(z_0, z_S, \phi)} \cdot (C_{\text{Veg}} \cdot \rho_{\text{Veg}}(\lambda) + (1 - C_{\text{Veg}}) \cdot \rho_{\text{Soil}}(\lambda)).$$

As proxy for the vegetation fraction the NDVI is used.

$$C_{\text{Veg}} = \text{NDVI}^* = \frac{\rho^*(0.865\,\mu\text{m}) - \rho^*(0.665\,\mu\text{m})}{\rho^*(0.865\,\mu\text{m}) + \rho^*(0.665\,\mu\text{m})} \tag{6}$$

with $\rho^* = \rho_{\text{TOA}} - \rho_{\text{Ray}} - \rho_{\text{Aer}}^{\text{Guess}}$ is taken from the NDVI*, the atmospherically corrected NDVI of the scene, and the scaling factor SF is used to adapt the spectrum to the radiation conditions in the scene

$$\text{SF} = \frac{\rho_{\text{TOA}}(0.665\,\mu\text{m}) - \rho_{\text{Ray}}(0.665\,\mu\text{m} - \rho_{\text{Aer}}^*(0.665\,\mu\text{m})}{C_{\text{Veg}} \cdot \rho_{\text{Veg}}(0.665\,\mu\text{m}) + (1 - C_{\text{Veg}}) \cdot \rho_{\text{Soil}}(0.665\,\mu\text{m})}. \tag{7}$$

Since ρ^* requires a first guess of the aerosol reflectance, an estimate from channel 1 (0.412 μm) is used, assuming a "black" surface. This gives a first overestimated guess of AOT, since surface reflectance decreases with decreasing wavelength. This AOT is transferred to the channel 0.665 μm, using Angström power law with an exponent of 1 and giving the estimate of the aerosol reflectance for this channel.

The surface model of Eq. 6 is used in Eq. 2 for the determination of the aerosol reflectance from satellite data. The spectra of both surface types "green vegetation" and "bare soil" are shown in Figure 4. Averages measured data of the LACE-98 experiment (Ansmann et al., 2002, von Hoyningen-Huene et al., 2003) have been combined with measurement of the AVIRIS instrument (Airborne Visible/Infrared Imaging Spectrometer of NASA) to cover the whole spectral range. Figure 4 also indicates the high variability of soil. Bright soil decreases the sensitivity to aerosol, thus the retrieval is more restricted or even impossible.

Over ocean and in the NIR the Fresnel reflectance of the surface is sufficient to be considered, as one can see in Figure 4. However, for the SW channels water leaving and ocean surface reflectance is required. For SeaWiFS – because of the sensor tilt away from sun – a calculation of the ocean surface reflectance, using Cox and Munk (1954) with the actual geometry conditions of the scenes, is used and is sufficient to correct glint effects. For MERIS this is not sufficient, there glint regions needs to be excluded.

The correct estimation of the surface term by the spectral surface model is very important, because it determines directly the accuracy of AOT. A deviation of surface reflectance of 0.01 leads to a change in AOT depending on aerosol type of about 0.1.

The sensitivity of the aerosol reflectance with respect to deviations of the surface reflectance is shown in Figure 5. In case that the determination of surface reflectance by the model, Eq. (6) and the iteration described later in 3.5 lead to the apparent effective surface reflectance of the scene, the aerosol reflectance can be obtained with an accuracy of 0.005 and then the AOT depends on the selected look-up-tables (LUT). The adaptation of the apparent surface reflectance to that situation within the pixel and the minimization of the deviation between the estimation and the real situation is made by three parameters: (a) the scaling factor SF (Eq. 8), adapting the general level of the surface reflectance to radiance level within the scene, (b) the atmospheric corrected NDVI, giving the spectral behaviour of the surface reflectance for the short wave channels and (c) iterative smoothing of the AOT output, making a fine tuning with Eq. (15), described later in 3.5. Thus, the deviations of the apparent surface reflectance with the existing one should come close to 0. Additionally, the aerosol retrieval is made over areas with fully or partly vegetation cover. There, the expected reflectance for the channels 1–7 is in the range of

11

0.05 and less. Thus, good conditions for the aerosol retrieval exist.

3.4 AOT determination

For the conversion of the reflectance data into AOT look-up-tables (LUT) either between top-of-atmosphere reflectance and AOT or aerosol reflectance and AOT are required. For the generation of LUT radiative transfer model calculations have to be performed, using aerosol and surface characteristics, Rayleigh scattering and geometry of illumination and observation. Aerosol characteristics are given by an aerosol phase function, the spectral single scattering albedo and a range of AOT, for instance 0.03–2.5. Since the observation data are corrected to an aerosol reflectance, also the radiative transfer calculations are corrected in the same way:

$$\rho_{\mathrm{Aer}}(\lambda) = \rho_{\mathrm{TOA}}(\lambda) - \rho_{\mathrm{Ray}}(\lambda) - \frac{t_{tot}(z_0) \cdot t_{tot}(z_S) \cdot A_{\mathrm{Surf}}(\lambda)}{1 - A_{\mathrm{Surf}}(\lambda) \cdot r_{\mathrm{hem}}(\delta_{\mathrm{tot}}, g)}. \tag{8}$$

Since in this case $\rho_{\mathrm{Ray}}(\lambda)$ and $\rho_{\mathrm{Surf}}(\lambda)$ are known, $\rho_{\mathrm{Aer}}(\lambda)$ starts at 0.0 for AOT=0 and contains multiple scattering exchange between aerosols and air molecules. Thus the LUTs contain AOT as functions of aerosol reflectance.

$$\delta_{\mathrm{Aer}}(\lambda) = f(\rho_{\mathrm{Aer}}(\lambda, z_0, z_S, \phi)) \tag{9}$$

For each geometry constellation and spectral channel one obtains functions, which can be parameterised as polynomials of the second degree:

$$\delta_{\mathrm{Aer}}(\lambda) = c_0(\lambda, z_0, z_S) + c_1(\lambda, z_0, z_S) \cdot \rho_{\mathrm{Aer}}(\lambda, z_0, z_S) + c_2(\lambda, z_0, z_S) \cdot \rho_{\mathrm{Aer}}^2(\lambda, z_0, z_S), \tag{10}$$

resulting in sets of c_0, c_1 and c_2 coefficients for each geometry constellation and spectral channel. The polynomial fit enables a fast interpolation between the discrete values of the radiative transfer modeling. Thus for each channel the AOT δ_{Aer} will be retrieved.

Since this is a quite large number of cases a reduction of cases is made, using air mass corrected aerosol reflectance ($\rho_{\mathrm{Aer\_AC}}$). For these corrections single scattering in the atmosphere is assumed.

$$\rho_{\mathrm{Aer\_AC}} = \rho_{\mathrm{Aer}} \cdot \frac{M(z_0) + M(z_S)}{M(z_0) \cdot M(z_S)} \tag{11}$$

12

These air mass corrected LUT reduce the number of required relationships to few ones for reference air mass conditions, which also will parameterized in form of polynomials of second degree for a fast processing. As one can see from Figure 7 this simplification gives quite good approximation for AOT <1. For AOT > 1 the deviations due to multiple scattering require the correct consideration of the geometry conditions. However, the most situations fulfil the first condition.

Figure 6 gives a graphical example of the LUT content by plotting AOT as function of the aerosol- or TOA reflectance, computed using "green vegetation" as surface, for non absorbing aerosol and for an experimental aerosol phase function, determined during the LACE-98 experiment.

The aerosol characteristics of the radiative transfer calculations for the LUT are the phase function, spectral single scattering albedo and a given range of AOT (like here, 0–2.5). The phase function and single scattering albedo are obtained either of predefined aerosol models, like OPAC (Hess et al., 1998) or experimental data of sun-/sky radiometer measurements of AERONET (Dubovik et al., 2000, 2002, 2006,) or special campaigns, like ACE-2, LACE-98, SAMUM (von Hoyningen-Huene et al., 1997, 1999a, 1999b, 2003, 2009, Silva et al., 2002, Ansmann et al., 2002). Aerosol phase functions and single scattering albedo, applied in radiative transfer calculations for LUT are presented in Figures 8 and 9.

The main characteristics of the aerosol for the LUT are the phase functions. They are normalized to 1 (in 1/sr). The spectral change in phase function is neglected within the wavelength range of 0.412–0.670 μm for the land retrievals, because experimentally no significant deviations could be found. Also the spectral change in single scattering albedo is neglected, because it is small in the used spectral range. The set of selectable LUT of BAER is presented in Table 3.

The application of the algorithm with several test scenes, using different LUT and the validation lead to the conclusion, that LUT No. 6, LACE-98, non-absorbing aerosol worked as an all round LUT, giving close results with AERONET data for the most conditions.

In cases of strong pollution high AOT tend to be underestimated up to 20% with this LUTs. Therefore LUTs with more absorbing aerosol need to be selected.

13

Applying LUT with the first guess of aerosol reflectance, obtained by the corrections of Rayleigh path reflectance and surface reflectance as described in Sect. 3.3, gives an AOT with a noisy spectral behaviour, varying around the real spectral slope. The spectral AOT obtained has no smooth decreasing spectral behaviour as it should be according to aerosol models. It has over land a noisy disturbed spectral slope, which disables a clear determination of an aerosol type from the 7 channels of the MERIS observation. Therefore an iterative smoothing of the spectral behaviour of the AOT with an application of convergence criteria is required.

3.5 Constraints, iterative smoothing and convergence criteria for AOT

Since in the reality the aerosol optical thickness has a smooth spectral behaviour, the noisy disturbed spectral slope, obtained by the application of Eq. (2) and (10), is constrained to follow approximately an Angström power law

$$\overline{\delta_{\text{Aer}}}(\lambda) = \beta \cdot \lambda^{-\alpha} = \delta_{\text{Aer}}(\lambda_{\text{ref}}) \cdot (\frac{\lambda}{\lambda_{\text{ref}}})^{-\alpha}. \tag{12}$$

One could use also another spectral aerosol model. However, the information content of the satellite data is not sufficient to separate more sophisticated aerosol models from surface effects without interferences of surface effects. Therefore we selected this simple spectral model for smoothing.

The deviations determined from the individual estimates $\delta_{\text{Aer}}(\lambda_\iota)$ of channel i and the value $\overline{\delta_{\text{Aer}}}(\lambda_i)$ represented by the Angström power law should be minimized, expressed by the

$$\text{RMSD} = \frac{1}{N}\sqrt{\sum_{i=1}^{N}(\delta_{\text{Aer}}(\lambda_i) - \overline{\delta_{\text{Aer}}}(\lambda_i))^2} \tag{13}$$

by modifying the surface reflectance in an iterative scheme running over j,

$$\rho_{\text{Surf},j}(\lambda) = \rho_{\text{Surf},j-1}(\lambda) \cdot w(\lambda) \cdot (1 - \frac{(\delta_{\text{Aer},j}(\lambda) - \overline{\delta_{\text{Aer},j}}(\lambda))}{\delta_{\text{Aer},j}(\lambda)}). \tag{14}$$

until root mean square deviation, RMSD < 0.005 is reached.

14

Here are $\beta = \delta_A(\lambda = 1.0\,\mu m)$, the turbidity coefficient and α the spectral slope of Angström power law. Instead of β another reference wavelength λ_{ref} for the reference AOT can be used, which is in this case the AOT of the first instrument channel. This is connected with the lowest surface reflectance and therefore the lowest retrieval error by the surface influence. The weighting factors $w(\lambda)$ determine the degree of variation of the surface reflectance spectrum by the iterations and determine the speed of the convergence. Small values will be used for reflectance values close to the expected ones and large values for channels with expected larger deviations.

The Angström parameters α and β are calculated here by the least squares fit of the Angström power law with the retrievals for all used spectral channels, i.e. channels 1 to 7 over land, instead of the mostly applied two-channel-approaches, cf. Eck et al. (1999).

With this fit, we get:

$$\alpha = \frac{\sum_{i=1}^{N}\left[(\ln\delta_{Aer}(\lambda_i) - \overline{\ln\delta_{Aer}}) \cdot (\ln\lambda_i - \overline{\ln\lambda})\right]}{\sum_{i=1}^{N}[\ln\lambda_i - \overline{\ln\lambda}]^2)} \tag{15}$$

and

$$\beta = \exp(\overline{\ln\delta_{Aer}} + \overline{\ln\lambda} \cdot \alpha) \tag{16}$$

with N – the number of spectral channels used.

$\overline{\ln\delta_{Aer}} = \frac{1}{N}\sum_{i=1}^{N}\ln\delta_{Aer}(\lambda_i)$ and $\overline{\ln\lambda} = \frac{1}{N}\sum_{i=1}^{N}\ln\lambda_i$ describe the averaged logarithms of the spectral AOT and wavelengths, respectively.

This approach gives a much more stable estimation of the Angström parameters for a multi-wavelength approach then a two-wavelength estimation, especially, if one has errors in the first iterations for the AOT of the single channels. Furthermore it is easy to transfer the reference wavelength for the AOT from $\beta = \delta_{Aer}$ (1.0 μm) to each wavelength desired, using Eq. (13). The main purpose of the use of the Angström power law is to ensure a sufficient smoothness of the AOT spectrum.

For the first iteration of the determination of the AOT, the surface reflectance obtained by Eq. (6) is used. Then, the iterative smoothing described in Eq. (15) modifies the spectral surface reflectance depending on deviations of the smoothed spectral AOT. With the modified

15

surface reflectance an improved AOT is obtained and so on, until RMSD has reached its defined minimum. Finally the AOT for the used spectral channels is found and the iteration can be stopped.

Within the iterations the Angström parameters are constrained as follows: The spectral slope α is determined in the first iteration from the retrieved value of the AOT. It is defined to lie within the limits $-0.5 \leq \alpha \leq 2.0$. These boundaries are selected from extreme spectral conditions for the AOT, found in ground-based measurements. If the retrieved spectral slope is outside this limit it is set to the climatologic average of $\alpha = 1.3$. This constraint corresponds to the range of the alpha obtained for the majority of atmospheric aerosol types from sunphotometer measurements (Holben et al., 2001) and models cf. d'Almeida et al.,1991.

Extensive applications of the procedure indicate a different impact of the different spectral channels on the determination of spectral slope of AOT. Since the MERIS channels 1 to 4 (0.412 - 0.510 m) with low surface reflectance enable to recognize the spectral slope, these channels are most important. Therefore these channels are treated with smaller weighting factors $w(\lambda)$ in Eq. (15) than channels 6 and 7 close to "the red edge". The weighting factor scales spectrally the iterative change of the surface reflectance, thus it determines the convergence of the iteration. The weighting factors were determined empirically to reach a fast enough and sufficiently stable convergence of the iteration procedure. In channel 5 at $0.560\,\mu m$ an insufficient separation of the vegetation peak is found. The vegetation peak at this wavelength is highly variable and this variability is not well considered by the linear mixing model of the spectral surface reflectance (Eq. 6) using one spectrum for "green vegetation" and "bare soil" only. This was the reason for increased AOT in this channel and consequently systematic decreased Angström α. Therefore this channel is associated with an increased weighting factor $w(\lambda)$.

3.6   Cloud screening in BAER

Very important for the retrieval of AOT are really cloud free conditions, because the approach described above, is valid for cloud free conditions only. Therefore a pre-step for the AOT retrieval is a rigorous cloud screening. Unconsidered clouds increase the retrieved AOT and change their spectral behaviour. This is very relevant, if temporal averages are required. One

non-recovered cloud can bias the average for one month significantly.

Since MERIS and SeaWiFS do not have channels in the thermal IR, the cloud screening uses cloud properties in the VIS channels of the instruments for their discrimination.

Based on main cloud properties: (1) clouds are bright, e.g. cloudy pixels have an increased TOA reflectance, (2) clouds have a spectrally neutral reflectance, (3) clouds are elevated and (4) clouds are inhomogeneous, three criteria for the cloud screening have been derived:

1. pixels are flagged as cloudy, if the TOA reflectance ρ_{TOA} in 3 SW channels exceeds the minimum cloud reflectance ρ_{Cl_Min}, following Kokhanovsky, 2001: $\rho_{TOA} \geq \rho_{Cl\_Min}$. For nadir conditions and normal aerosol loads is $\rho_{Cl\_Min} = 0.2$. This condition works for fully cloudy pixels. It has limits for strongly increased aerosol loading (strong urban pollution, desert dust storms, plumes of forest fires). In this case ρ_{Cl_Min} has to be increased. It is not sufficient for low fractional cloud coverage. For this purpose clouds should be "white" in a RGB plot, while aerosols deviate from "white".

2. a decreased spectral slope of TOA reflectance indicates thin clouds and fractional cloud coverage below ρ_{Cl_Min}. The characterization of the spectral slope is made by the ratio of channel 1 and 2: $R = \rho_{TOA} (0.412\,\mu m)/\rho_{TOA} (0.443\,\mu m)$. The analysis of this ratio for scenes over Europe for cloudy and cloud free scenes, one example is presented in Figure 10, leads to a ratio of 1.15. Therefore partly cloudy scenes will be removed from cloud free ones by using the criterion $R > 1.15$.

3. since clouds are inhomogeneous the ratio of standard deviation ($\sigma_{5\times5}$) to average of ρ_{TOA} ($AV(\rho_{TOA})_{5\times5}$) or AOT ($AV(AOT)_{5\times5}$) is used to characterize the spatial variability within a 5×5 pixel box for the retrieved spectral channels. If $R_V = \sigma_{5\times5}/AV > 0.10$, then a scene is taken as cloudy. For low AOT an increased boarder needs to be selected.

All three criteria together remove the most cloud effects. However, not all criteria can be applied everywhere and for every case. For instance, over bright desert ground ρ_{Cl_Min}, criterion 1 has to be increased. If bright grounds are elevated, R under criterion 2. needs to be decreased. A very low AOT (< 0.1) requires an increased R_V, because of heterogeneity of land surface. Therefore bright grounds, like snow and ice cover, also very bright bare soil regions are excluded.

18

Other effects, connected with clouds are cloud shadows. Cloud shadows cause too low AOT values (even sometimes a negative one). For the detection of cloud shadows two indicators can be applied.

1. One fraction of cloud shadows occur within areas of scattered clouds and increases the standard variation and will be removed by the analysis of the inhomogeneity (criterion 3).

2. Secondly cloud shadows reduce the atmospheric scattering and surface reflection. The case having a TOA reflectance lower than Rayleigh path reflectance, $\rho_{\mathrm{TOA}} < \rho_{\mathrm{Ray}}$, is a clear indication for cloud shadows.

Since the cloud products of standard satellite data products (like cloud fraction or cloud flagging) do not cover the case of totally cloud free sky in a sufficient way for an aerosol retrieval, the application of all criteria above for clouds and cloud shadows is recommended. The criteria above are investigated and tested within the MICROS approach for the determination of synergetic cloud fration algorithm, presented by Schlundt et al., 2010.

3.7 BAER versions

The approach described above exists in different realizations depending on instrument and input data products. Thus the program can be used for MERIS RR (reduced resolution) and MERIS FR (full resolution) data. Here all spectral MERIS channels are used, except those having strong gaseous absorption of O_2 (channel 11) and water vapour (channel 15)–13 channel version. Thus 7 channels below the "red edge" can be used for the determination of the spectral AOT (0.412–0.670 µm) and the NIR channel at 0.865 µm additionally is used additionally for the NDVI. Both versions extrapolate then the AOT for all MERIS channels and perform a complete atmospheric correction for them, giving additionally surface directed spectral reflectance. In the case of L1 data, the TOA radiance, given by the L1 product, is transferred into TOA reflectance and the BAER approach is used as described above.

In the case of L2 data, the Rayleigh corrected reflectance is used, given by the L2 data product. The L2 data product provided by ESA, do not contain the complete atmospheric correction

19

over land. The processing of the product considers only the Rayleigh path reflectance. In this case the step of correction of Rayleigh path reflectance is omitted in BAER. This version completes atmospheric correction over land for the L2 data and is available as a plug-in for the BEAM toolbox, provided by ESA, BEAM, 2007 .

A version running with a reduced channel setting can be applied for different satellite instruments, having the main channels of ocean colour instruments, e.g. 6 channels below the "red edge" and the 0.865 µm for the determination of NDVI – 8 channel version. It can be used for MERIS L1 RR, MERIS L1, FR, SeaWiFS LAC (local area cover), SeaWiFS GAC (global area cover). MODIS data can be used, if the first ocean colour channels do not reach saturation over land.

4   Results and validation

4.1   Results of AOT retrievals

For the demonstration of the capabilities of the approach, described above, some examples of AOT retrievals are shown. We concentrate here on results for channel 2 (0.443 µm), because this channel has a low retrieval error. All retrievals have been made with the same LUT, No. 6 of Table 3. This LUT is selected, if no specific a-priori knowledge of the existing aerosol type is known. It is found, that in the most cases this LUT gives reliable results, as can be seen in Sect. 4.2 on validation.

The selected scenes of MERIS data are part of validation data sets for the validation results in Sect. 4.2. They show cases of low aerosol loading over Eastern US (Fig. 11) and high ones during Greek fire season in 2007 (Fig. 12). More detailed explanations are given within the figure captions.

As single scene (about 8 min of MERIS data) – a part of one orbit can be processed with a normal desktop personal computer. Larger scenes need to be split into smaller parts for processing and composed from the fractions. Examples of composites of more scenes and orbits are presented in Fig. 13 and Fig. 21.

Scenes of SeaWiFS data are presented in Fig. 14 and Fig. 21, to demonstrate the capability of the 8 channel version of BAER. Fig. 14 shows aerosol transport from Eastern US to the Atlantic and Fig. 21 a global daily composite of an AOT retrieval, using SeaWiFS GAC data.

Further a normal case of aerosol loading over Germany is selected in Fig. 15 to present spectral AOT and surface reflectance data of the retrieval in Fig. 16.

The selected scenes should give examples, how the approach can be applied for the observation of the regional aerosol impact in terms of the AOT as well over land as over ocean. Thus such aerosol retrievals can contribute to environmental control of air pollutions by aerosols, especially, if additional aerosol products, like PM10 concentrations are derived from AOT, as it is done in von Hoyningen-Huene et al., 2008.

Pollution in the valley of the river Po in northern Italy is visible. Increased AOT also can be seen in the vicinity of the large cloud system at the east side of the swath, probably caused by cloud influence.

The scene is used to present the retrieval data more in detail, e.g. spectral AOT and spectral surface reflectance in Fig. 16.

Rectangles indicate locations, where spectra of AOT have been selected. Three land sites, DK – Denmark (near Kolding), D – Germany (near Bremen), I – Italy (Po valley near Milan) have been selected, where AOT and surface reflectance is given. Additionally two sea sites have been selected for the spectra of surface reflectance: B – Baltic Sea and M – Mediterranean.

The spectral surface reflectance in Fig. 16b) is the result of the atmospheric correction, applying spectral AOT to correct for the effect of aerosol reflectance. The spectra over Denmark and Germany are typically for dark dense vegetation without free bare soil fractions. The spectra over Italy are typically for only fractional vegetation coverage, where the surface reflectance is partly determined by bare soil fractions.

4.2   Validation of AOT and error estimation

Validation and evaluation of the retrieval approach is made by different ways: (a) intercomparison of the AOT results with ground based AERONET data and (b) retrievals with synthetic test data, provided by Kokhanovsky et al., 2009.

(a) Inter-comparison with ground-based AERONET data.

For the BAER application with MERIS L1 data a validation against AERONET data has been made. Since the focus of our retrievals is mainly on Europe, 28 AERONET sites over Europe have been selected. Additional 9 sites in eastern US and Canada are included within this study. Fig. 17 indicates the positions of the validation sites, the names of the sites are provided in Table 5. Cloud screened level 2 (or if not available level 1.5) AERONET data have been used within a time $\pm$ 1 hour around the MERIS overflight time. Arbitrary cloud free MERIS scenes of different project studies and measurement campaigns within the time 2003 and 2006 have been used for comparisons with the ground-based data.

The retrieval procedure contains a data set with the geographic coordinates of the validation sites and within a circle of $0.03°$ around these coordinates. Average and standard deviation of AOT is taken from the retrieval results. This is compared with the ground based AOT data of the associated AERONET site within a time interval of $\pm$ 1 h. Since AERONET provides AOT data for the wavelength 0.44, 0.67, 0.87 and 1.02 µm, the first study was made with MERIS channel 2 (0.443 µm) in a direct inter-comparison.

The results of these inter-comparisons for the MERIS channel 2 (0.443 µm) are presented in Fig. 18.

The comparison of the retrieved AOT for the wavelength 0.443 µm with the AERONET channel of 0.440 µm in Fig. 18 shows, that both data sets are correlated. A significant relationship of retrieved AOT and AERONET is found as

$$\delta_{\text{Aer,MERIS}}(0.443\mu\text{m}) = 0.866 \cdot \delta_{\text{Aer,AERONET}}(0.440\mu\text{m}) + 0.051,$$

with a correlation coefficient of $r = 0.961$. The average deviation of the retrievals from the regression line for this data set is 0.052. Thus the retrieval error of AOT for the channel 0.443 µm can be estimated with $\Delta\delta_{\text{Aer}}(0.443\,\mu\text{m}) = \pm 0.05$. This is for an average AOT of 0.2 and error of 25%.

With a smaller data set the same study for MERIS channel 7 (0.665 µm) is made with AERONET channel of 0.67 µm over Europe only. Because of the lower AOT values the error of the retrieval is increased and the correlation is weaker. The correlation coefficient is $r = 0.832$ and the relative error reaches there 35%.

22

Since BRDF effects have a stronger effect on AOT for larger wavelengths than for shorter ones (increased surface reflectance and smaller AOT), the consideration of BRDF increases the Angström α parameter and leads to smaller AOT for the 0.665 µm wavelength. This could reduce the error for 0.665 µm. The effects of BRDF are still under investigation.

(b) Inter-comparison with synthetic test data

Simulated TOA reflectance data, obtained by SCIATRAN (Rozanov et al., 2001, 2005) have been provided by Kokhanovsky et al., 2009 for the test of aerosol retrieval algorithms. The modelled data of TOA reflectance were provided for conditions of "black" surface an "unknown" aerosol type and a given illumination and viewing geometry ($z_0 = 60°$, $z_S = 0°$) for a range of unknown values of AOT, which should be retrieved. Fig. 19 presents the results of AOT retrieval with the given AOT used for the radiative transfer modelling. The results of the inter-comparison give very different results. Using the LUT with the experimental LACE-98 phase function, which gave in the inter-comparison with the AERONET data the best results, a large underestimation of AOT has been obtained, using the modeled test data. Selecting the LUT for clean marine aerosol a quite good correspondence of the AOT retrieval has been found. The phase function of the clean marine model coincides with that phase function used for the modeling of synthetic TOA reflectance data. The phase functions used for the test retrievals and the synthetic data are plotted in Fig. 7. The different results underline the importance of the selection of the appropriate phase function in BAER. The disagreement of the retrieval results from the synthetic data, using LUT with the LACE-98 phase function, and on the other hand their quite good agreement with AERONET data, shows, that this synthetic data did not characterize the majority of real observation conditions.

4.3 First estimation of trends in AOT from SeaWiFS observations

The method described in Sect. 3 has been applied to the long-term data series of SeaWiFS Global Aerea Cover (GAC) data. The SeaWiFS data were available since October 1997 up to now. The presented and analysed here time span was October 1997–May 2008. The investigation of such a time span requires the consideration of the degradation of the SeaWiFS instrument, done by the SeaWiFS calibration team of NASA, providing the calibration func-

23

tions to calculate the radiance from the measured counts by the instrument. The degradation behaviour, given for the 5-th SeaWiFS reprocessing, is used, see examples for channel 2 and 8 in Fig. 20, to obtain a TOA reflectance free of degradation effects, which could be used then for the application with the BAER approach for the retrieval of AOT. One aerosol phase function (LUT number 6 from Table 3) is used for the whole time series. An example of the daily global aerosol product, which is used for the determination of monthly averages, is given in Fig. 21 for the 3 May 2006. An extended description of the trend determination and its validation will be given in Yoon et al., 2010. First results of long-term AOT retrieval for some of the regions of interest of the CITYZEN project (7. Framework Programme of the European Commission) are presented here. Selected regions of interest of this research program were under others: BeNeLux-big (Begium, Netherlands, Luxemburg and Rhein-Ruhr region of Germany: 1° E–8° E, 48° N–54° N), Po-Valley – big (Northern Italy: 7.5° E–13.5° E, 44° N–46° N), Eastern Europe (OECD definition, 18° E–60° E, 40° N–65° N) and Pearl River Delta (in China: 112° E–115.5° E, 22° N–24° N). All SeaWiFS observations of the regions have been used for the AOT retrieval of the SeaWiFS channels 1–6. Then monthly averages of AOT have been determined from the retrievals. The time series of the monthly averages of AOT for the four regions of interest are given in Fig. 22. The monthly averages of AOT show a distinct annual cycle, like also comparable AERONET data with increased AOT in summer month and lower values for winter. Fitting linear relationships through the retrieved monthly averages let estimate the average annual trend of AOT within the almost 11 year period. The obtained values for the trend are given in Table 6. Two channels (0.443 and 0.555 µm are presented. Differences in the trends for both wavelength are due to uncertainties, mainly in surface reflectance. The regions BeNeLux-big and Po-Valley-big show a clear negative trend in AOT over the period of 11 years connected with improved air quality within these regions. In the region Eastern Europe within the period almost no trend can be detected. However the region Paerl River Delta in China is characterized by a clear increasing trend of AOT. More results and investigation of the significance of the trends will be given by Yoon et al., 2010.

24

5 Summary and conclusions

conclusions

Bremen AErosol Retrieval (BAER) is a retrieval approach for AOT over land (and ocean) applicable for nadir viewing ocean colour sensors, like MERIS or SeaWiFS. It separates the spectral aerosol reflectance from surface and Rayleigh path reflectance for the short wave range of the measured spectrum of top-of-atmosphere reflectance less than $0.670\,\mu m$. The advantage of MERIS is the existence of several spectral channels in the blue and visible range enabling the spectral determination of AOT in 7 channels (0.412–$0.670\,\mu m$) and additionally channels in the NIR, which can be used to characterize the surface properties. A dynamical spectral surface reflectance model for different surface types is used to obtain the spectral surface reflectance for this separation. Normalized differential vegetation index (NDVI), taken from the satellite observations, is the model input. Spectral AOT is obtained from aerosol reflectance using look-up-tables, obtained from radiative transfer calculations with given aerosol phase functions and single scattering albedo either from aerosol models, given by OPAC or from experimental campaigns.

Validations of the obtained AOT retrieval results with AERONET data over Europe gave a preference for experimental phase functions derived from sky radiometer almucantar measurements. The validation showed an agreement of AOT with AERONET within 0.05. Further the retrieved AOT do not have sharp contrasts between land and ocean. Thus regional or temporal changes in AOT can be investigated. Using SeaWiFS data trends in AOT for specific regions could be found.

The ocean part of the retrieval approach is not described here. It uses a mixing of "clean water" and "coastal water", tuned by the NDPI (Normalized Differential Pigment Index). For the case of ocean water all channels of MERIS are included.

Separation of angular light field between surface (BRDF) and atmospheric (aerosol and Rayleigh phase function) effects is one of the major error sources for the AOT retrieval over land. The BRDF influence is still under investigation.

Additionall products, based on AOT can be derived. Necessary condition is an accurate retrieval of the spectral AOT. Thus Kokhanovsky et al. (2006) and von Hoyningen-Huene et al. (2008) estimated PM10 concentrations and effective radius from satellite data, using AOT and Angström α parameter.

References

references

d'Almeida, G. A., Koepke, P., and Shettle, E. P.: Global climatology and radiative characteristics, Deepak, Hampton. 561 pages, 1991.

Ansmann, A., U. Wandinger, A. Wiedensohler, and U. Leiterer, Lindenberg Aerosol Characterization Experiment 1998 (LACE 98): Overview, J. Geophys. Res., 107(D21), 8129, doi:10.1029/2000JD000233, 2002.

BEAM: Beam web-page, URL http: envisat.esa.int/services/beam/, 2007

Bezy, J.-L., Deelwart, S., and Rast, M.: Meris – a new generation of ocean colour sensor onboard Envisat. Technical report EAS Bulletin 103 (2000) 48–56, ESA, 2000.

Buchholz, A.: Rayleigh scattering calculations for the terrestrial atmosphere, Appl. Opt., 34, 2765–2773, 1995.

Delwart, S., Bourg, L., and Huot, J. P.: MERIS 1st year: Early calibration results, Proceedings of the International Society for Optical Engineering (SPIE): Sensors, Systems and Next-Generation Satellite VII, Barcelona, Spain vol. 5234, pp. 379–390, 2003.

Dinter, T., von Hoyningen-Huene, W., Burrows, J.P., Kokhanovsky, A., Bierwirth, E., Wendisch, M., Mller, D., Kahn, R. and Diouri, M.: Retrieval of aerosol optical thickness for desert conditions using MERIS observations during SAMUM campaign. Tellus 61B (2009), 220–237, 2009

Dubovik, O. and King, M. D.: A flexible inversion algorithm for retrieval of aerosol optical properties from sun and sky radiance measurements, J. Geophys. Res., 105, 20673–20696, 2000.

Dubovik, O., Holben, B. N., Lapyonok, T., Sinyuk, A., Mishchenko, M. I., Yang, P., and Slutsker, I.: Non-spherical aerosol retrieval method emploing light scattering by sheroids, Geophys. Res. Lett., 29(10), 1415, doi:10.1029/2001GL014506, 2002.

Dubovik, O., Sinyuk, A., Lapyonok, T., Holben, B. N., Mishchenko, M., Yang, P., Eck, T. F., Volten, H., Munoz, O., Veihelmann, B., van der Zande, W. J., Leon, J.-F., Sorokin, M., and Slutsker, I.: Application of spheroid models to account for aerosol particle nonsphericity in remote sensing of desert dust, J. Geophys. Res., 111, D11208, doi:10.1029/2005JD006619, 2006.

Eck, T. F., Holben, B. N., Reid, J. S., Dubovik, O., Smirnov, A., O'Neill, N. T., Slutsker, I., and Kinne, S.: Wavelength dependence of the optical depth of biomass burning, urban and desert dust aerosols, J. Geoph. Res., 104, 31333–31349, 1999.

GCOS - Systematic observation requirements for satellite-based products for climate. GCOS -107, Sept. 2006, WMD/TD No.1338. http://www.wmo.int/pages/prog/gcos/Publications/gcos-107.pdf

GTOPO-30, USGS product page: http://eros.usgs.gov/\#/Find_Data/Products_and_Data_Available/gtopo30_info

Hess, M., Koepke, P., and Schult, I.: Optical properties of aerosols and clouds: The software package OPAC, Bull. Am. Met. Soc., 79, 831–844, 1998.

Holben, B. N., Tanré, D., Smirnov, A., Eck, T. F., Slutsker, I., Abuhassan, N., Newcomb, W. W., Schafer, J. S., Chatenet, B., Lavenu, F., Kaufman, Y. J., de Castle, J. V., Setzer, A.,Markham, B., Clark, D., Froin, R., Halthore, R., Karnieli, A., O'Neill, N. T., Pietras, C., Pinker, R. T., Voss, K., Zibordi, G.: An emerging ground-based aerosol climatology: Aerosol optical depth from AERONET, J. Geoph. Res., 106, 12067–12097, 2001.

Hsu, N. C., Tsay, S.-C., King, M. D., and Herman, J. R.: Aerosol Properties Over Bright-Reflecting Source Regions, IEEE, Trans. Geos. Rem. Sens., 42, 557–569, 2004.

Martiny, N., Santer, S., and Smolskaia, I.: Vicarious calibration of MERIS over dark waters in the near infrared, Remote Sens. Environ., 94, 475–490, 2005a.

27

Martiny, N., Frouin, R., and Santer R.: Radiometric calibration of SeaWiFS in the near infrared, Appl. Opt., 44(36), 7828–7844, 2005b.

Kaufman, Y. J., Tanré, D., Gordon, H. R., Nakajima, T., Lenoble, J., Frouin, R., Grassl, H., Herman, B. M., King, M. D., and Teillet, P. M.: Passive remote sensing of tropospheric aerosol and atmospheric correction for the aerosol effect, J. Geophys. Res., 102, 16815–16830, 1997.

Kaufman, Y. J., Tanré, D., Remer, L. A., Vermote, E. F., Chu, A., and Holben, B. N.: Operational remote sensing of tropospheric aerosol over land from EOS moderate resolution imaging spectrometer, J. Geophys. Res., 102, 17051–17067, 1997.

Kokhanovsky, A. A.: Reflection and transmission of polarized light by optically thick weakly absorbing random media, J. Opt. Soc. Am., 18, 883–887, 2001.

Kokhanovsky, A. A., von Hoyningen-Huene, W., and Burrows, J. P.: Atmospheric aerosol load from space, Atmos. Res., 81, 176–185, 2006.

Kokhanovsky, A. A. and de Leeuw, G.: Aerosol remote sensing over land. Springer Praxis, Chichester, 387 p., 2009.

Kokhanovsky, A. A., Deuzé, J. L., Diner, D. J., Dubovik, O., Ducos, F., Emde, C., Garay, M. J., Grainger, R. G., Heckel, A., Herman, M., Katsev, I. L., Keller, J., Levy, R., North, P. R. J., Prikhach, A. S., Rozanov, V. V., Sayer, A. M., Ota, Y., Tanré, D., Thomas, G. E., and Zege, E. P.: The inter-comparison of major satellite aerosol retrieval algorithms using simulated intensity and polarization characteristics of reflected light, Atmos. Meas. Tech. Discuss., 2, 3369–3439, 2009.

Maignan, F., Breòn, F.-M., and Lacaze, R.: Bidirectional reflectance of Earth targets: valuation of analytical models using a large set of spaceborne measurements with emphasis on the Hot Spot, Remote Sens. Environ., 90, 210–220, 2004.

Rozanov, V. V., Buchwitz, M., and Burrows, J. P.: SCIATRAN – A new radiative transfer model for geophysical applications in the 240–2400 nm spectral region: The pseudo.spherical version, Adv. Space Res., 29, 1831–1835, 2001.

Rozanov, A. A., Rozanov, V. V., Buchwitz, M., Kokhanovsky, A. A., Burrows, J. P.: SCIATRAN 2.0 – a new radiative transfer model for geophysical applications in the 175–2400 nm spectral range, Adv. Space Res., 36, 1015–1019, 2005.

Schlundt, C., Kokhanovsky, A.A., von Hoyningen-Huene, W., Dinter, D., Istomina, L., Burrows, J.P.: Synergetic cloud fraction determination for SCIAMACHY using MERIS. AMTD, 3, 3601–3642, 2010. doi:10.5194/amtd-3-3601-2010. http://www.atmos-meas-tech-discuss.net/3/3601/2010/

Silva, A. M., Bugalho, M. L., Costa, M. J., von Hoyningen-Huene, W., Schmidt, T., Heintzenberg, J., and Henning, S.: Aerosol optical properties from columnar data during the second

Aerosol Characterization Experiment an the south coast of Portugal. JGR 107 (2002) D22, 4642, doi:10.1029/2002JD002196, 2002.

Treffeisen, R., Tunved, P., Ström, J., Herber, A., Bareiss, J., Helbig, A., Stone, R. S., Hoyningen-Huene, W., Krejci, R., Stohl, A., and Neuber, R.: Arctic smoke - aerosol characteristics during a record smoke event in the European Arctic and its radiative impact, Atmos. Chem. Phys., 7, 3035–3053, 2007.

von Hoyningen-Huene, W., Freitag, M., and Burrows, J. B.: Retrieval of aerosol optical thickness over land surfaces from top-of-atmosphere radiance, J. Geophys. Res., 108(D9) 4260, doi:10.1029/2001JD002018, 2003.

von Hoyningen-Huene, W. A., Kokhanovsky, A., Burrows, J. P., Bruniquel-Pinel, V., Regner, P.: Simultaneous Determination of Aerosol- and Surface Characteristics from Top-of-Atmosphere Reflectance using MERIS on board of ENVISAT, J. Adv. Space Res., 37, 2172–2177, 2006.

von Hoyningen-Huene, W. and Posse, P.: Non-sphericity of Aerosol Particles and Their Contribution to Radiative Forcing, J. Quant. Spectr. Rad. Trans., 57, 651–668, 1997.

von Hoyningen-Huene, W., Wenzel, K., and Schienbeinm, S.: Radiative Properties of Desert Dust and its Effect on Radiative Balance, J. Aeros. Sci., 30, 489–502, 1999.

von Hoyningen-Huene, W., Schmidt, T., Schienbein, S., Chan, A. K., and Lim, J. T.: Climate relevant aerosol parameters of South-East Asian forest fire haze, Atmos. Environ., 33, 3183–3190, 1999.

von Hoyningen-Huene, W., Kokhanovsky, A. A., and Burrows, J. P.: Retrieval of Particulate Matter from MERIS Observations, in: Advanced Environmental Monitoring, edited by: Kim, J. Y. and Platt, U., Springer, 190–202, 2008.

Yoon, J. M., von Hoyningen-Huene, W., Vountas, M., and Burrows, J. P.: Analysis of long-term trend of aerosol optical thickness using Bremen AErosol Retrieval algorithm with SeaWiFS data over regions of interest, ACP, submitted, 2010.

29

Table 1. Spectral channels of MERIS and SeaWIFS.
table

MERIS		SeaWiFS		Remarks
Channels	15	Channels	8	
Wavelength (μm)	Band width (μm)	Wavelength (μm)	Band width (μm)	
0.4127	0.00994	0.412	0.02	AOT(L)
0.4426	0.00995	0.443	0.02	AOT(L)
0.4899	0.00996	0.490	0.02	AOT(L)
0.5098	0.00996	0.510	0.02	AOT(L)
0.5597	0.00997	0.555	0.02	AOT(L)
0.6196	0.00998			AOT(L)
0.6646	0.00999	0.670	0.02	AOT(L,O),NDVI
0.6808	0.00749			
0.7083	0.00999			
0.7534	0.00750			AOT(O)
0.7615	0.00374			O_2-A absorption
0.7784	0.01501	0.765	0.04	AOT(O)
0.8648	0.02004	0.865	0.04	AOT(O)NDVI
0.8849	0.01001			AOT(O)
0.9000	0.01002			H_2O

Table 2. Observation characteristics of the instruments.

Instrument	Swath width (km)	Spatial resolution (km^2)	Coverage	Repetition time (days)
MERIS				
RR mode	1100	1.1×1.1	Global	2–3
FR mode	1100	0.3×0.3	Europe	
SeaWiFS				
LAC mode	2801	1.1×1.1	Receiving stations	1
GAC mode	1502	4.5 x 4.5	Global	1–2
MODIS				
1 km agglom.	2330	1×1	Global	1

31

Table 3. Look-up-tables in use and their characteristics.

LUT Number	Aerosol Model	Phase function	Single scattering albedo ($\lambda = 0.5\,\mu\text{m}$)
1	Clean marine	OPAC, clean marine	1.0
2	Clean continental	OPAC, clean continental	0.975
3	Average continental	OPAC, average continental	0.928
4	ACE-2, marine	ACE-2, experimental	1.0
5	LACE-98, absorbing	LACE-98, experimental	0.98
6	LACE-98, non-abs.	LACE-98, experimental	1.0
7	Desert	SAMUM, experimental	0.97

32

Table 4. Overview of BAER versions.

Input data	BAER Version	Results	Remarks
MERIS L1 RR	13 channel version	AOT for MERIS channel 1–7 Surface reflectance for channel 1–10, 12–14	Spatial resolution 1.1×1.1 km^2
MERIS L1 FR	13 channel version	AOT for MERIS channel 1–7 Surface reflectance for channel 1–10, 12–14	Spatial resolution 0.3×0.3 km^2, same program as above
MERIS L1 RR SeaWiFS LAC (MODIS)	8 channel version	AOT for MERIS channel 1–5, 7 or SeaWiFS channel 1–6	Spatial resolution 1.1×1.1 km^2
SeaWiFS GAC	8 channel version	AOT for SeaWiFS channel 1–6	Spatial resolution 4.5×4.5 km^2
MERIS L2 RR	13 channel version	AOT for MERIS channel 1–7 Surface reflectance for channel 1–10, 12–14	Spatial resolution 1.1×1.1 km^2, completion of atmospheric correction of MERIS L2 product over land

33

Table 5. AERONET sites used in validation studies of BAER

Europe Location	Lat.	Lon.	North America Location	Lat.	Lon.	Other regions Location	Lat.	Lon.
Avignon	43.933	4.878	Cartel X	45.379	-71.931	Anmyon	126.267	126.267
Dunkerque	51.035	2.368	Columbia SC	34.023	-81.036	Ascension	-7.883	-14.417
Bremen (IUP Cimel)	53.05	8.78	Cove	36.900	-75.710	Azores	38.530	-28.630
Cabauw	51.971	4.927	Egbert	44.226	-79.750	Bamizoubou	13.541	2.665
DenHaag	52.110	4.327	GSFC	39.030	-76.880	Cabo$_{Verde}$	16.733	-22.935
Dunkerque	51.035	2.368	MD Science Center	39.283	-76.618	Ilorin	8.320	4.340
El-Arenosillo	37.105	-6.733	Walker Branch	35.958	-84.284	Midway	28.220	-177.170
Evora	38.568	-7.912	Wallops Island	37.942	-75.475	Ouagadogou	12.200	-1.400
Fontaibleau	48.407	2.680				Praja	14.974	-23.484
Ft. Crete	34.656	22.129				SantaCruz	28.660	-16.330
Gotland	57.917	18.950				Thala	35.550	8.683
Hamburg	53.586	9.973						
Helgoland	54.178	7.887						
ISGDM-CNR	45.437	12.332						
Ispra	45.803	8.627						
Karlsruhe	49.093	8.428						

Europe (continued)						Europe (continued)		
Laegeren	47.480	8.351				Oristano	40.307	7.906
Lampedusa	35.517	12.632				Palaiseau	48.700	2.208
Lecce	40.335	18.111				Paris	48.867	2.333
Leipzig	51.354	12.435				Rome	41.840	12.647
Lille	50.612	3.142				Stockholm	58.580	16.150
Mainz	49.999	8.300				Toravere	58.255	26.468
Messina	38.197	15.567				Toulon	43.136	6.009
Modena	44.632	10.945				Venise	45.314	12.508
Oostende	51.225	2.925						

Table 6. Average annual change in AOT for selected regions of interest.

Wavelength/ Region	Channel 1, 0.412 μm ΔAOT(0.412)/year	Channel 5, 0.555 μm ΔAOT(0.555)/year
BeNeLux-big	-0.0039	-0.0034
Po-Valley-big	-0.0033	-0.0031
Eastern Europe	-0.00055	-0.00013
Pearl River Delta	$+0.0065$	$+0.0044$

Fig. 1. Main spectral properties of land and ocean surface and its TOA reflectance. Left: land conditions with continental aerosol, right: ocean conditions with clean marine aerosol. Restrictions for the aerosol retrieval over land arise from increase of surface reflectance due to the "red edge" ($\lambda > 0.67\,\mu m$) and an increased variability of surface reflectance by the chlorophyll peak at $0.55\,\mu m$.

figure

Fig. 2. Scheme of the main steps of BAER and its interactions.

Fig. 3. Relative BRDF calculated for two illumination conditions (solar zenith 22.39° and 63.11°) and the viewing range of MERIS for different parameters of the RPV model, used in the VIS channels.
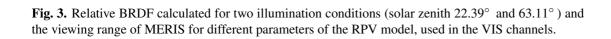
Fig. 4. Main surface reflectance spectra used for the surface reflectance model such as "green vegetation" and "bare soil" in comparison with experimental data. The high reflectance of bright soil causes additional restrictions for the aerosol retrieval.

39

Fig. 5. Sensitivity of aerosol reflectance $\rho_{\mathrm{Aer}}(\lambda)$ against deviations of surface reflectance $\rho_{\mathrm{Surf}}(\lambda)$ from true value for selected geometry conditions.
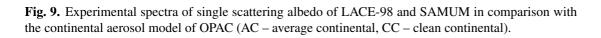
Fig. 6. Examples of spectral look-up-tables to convert a) left: TOA reflectance to AOT and b) right: aerosol reflectance into AOT for the main MERIS channels for one given illumination – viewing configuration ($z_0 = 38°$, $z_S = 23°$, $\phi = 68°$). The example shows results for LUT No. 6 – experimental phase function of LACE-98 and non absorbing aerosol.

Fig. 7. Dependence of AOT from aerosol reflectance for MERIS channel 2 (0.443 μm). Influence of illumination and viewing geometry on LUT (left) and after its airmass correction (right).

Fig. 8. Experimental phase functions of the experiments, ACE-2, LACE-98 and SAMUM in comparison with phase functions of the OPAC aerosol models, which are used for the LUT calculation. Additionally the dashed line gives the phase function for the synthetic data of the algorithm inter-comparison by Kokhanovsky et al., 2009.

Fig. 9. Experimental spectra of single scattering albedo of LACE-98 and SAMUM in comparison with the continental aerosol model of OPAC (AC – average continental, CC – clean continental).

Fig. 10. Example of a histogram of the ratio $R = \rho_{\text{TOA}}$ $(0.412\,\mu\text{m})/\rho_{\text{TOA}}(0.443\,\mu\text{m})$ of a real satellite scene. The ratio value, discriminating the clear sky range is used for cloud screening.
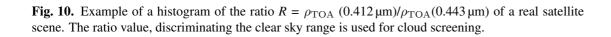
Fig. 11. Retrieval of AOT for 0.443 μm of a clear day over eastern US for 21 November 2003, 15:48 UTC. Clearly aerosol source regions can be identified. New York, Philadelphia, Washington and some other urban areas in Florida can be identified with an increased AOT of about 0.07×0.1 compared with the surrounding conditions. Near the South-East coast of Florida disturbances from "case 2" – water with sediment content can be seen as apparently increased AOT.

46

Fig. 12. Smoke plumes of the large forest fires in Greece of summer 2007, MERIS RR scene of 26 August 2007, 09:21 UTC. Several forest fires at the Greek and Albanian coast can be identified and the aerosol transport along the trajectories to the south – west can be observed. Thus satellite observations enable the control of pollution even there, where no direct observations are available.

47

Fig. 13. Composite of MERIS AOT retrievals for the wavelength 0.443 μm of 3 orbits of MERIS RR data over northern Europe for 1 May 2006, showing pollution transport around a high pressure system over northern Russia. The scene shows a large scale pollution transport from Europe to the Arctic, causing arctic haze. The atmospheric conditions and the study of pollution transport is discussed in detail in Treffeisen et al., 2007. The highest values of AOT in the pollution plume over Russia are screened out by the cloud screening, also scattered clouds are not removed totally, because not all criteria of the cloud screening have been applied.

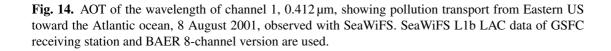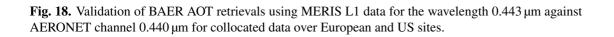**Fig. 14.** AOT of the wavelength of channel 1, 0.412 µm, showing pollution transport from Eastern US toward the Atlantic ocean, 8 August 2001, observed with SeaWiFS. SeaWiFS L1b LAC data of GSFC receiving station and BAER 8-channel version are used.

49

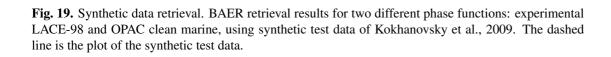**Fig. 15.** Retrieval of AOT for 0.443 µm over Germany and surrounding areas, using MERIS RR L1 data of 13 October 2005, 09:54 UTC, showing average autumnal aerosol loading. Pollution in the valley of the river Po in northern Italy is visible. Increased AOT also can be seen in the vicinity of the large cloud system at the east side of the swath, probably caused by cloud influence.

Fig. 16. **(a)** – left – retrievals of spectral AOT of the MERIS RR scene of 13 October 2005, 09:54 UTC for the selected regions in Fig. 14: Denmark (near Kolding), Germany (near Bremen), Italy (Po valley near Milan). **(b)** – right – spectral surface reflectance for all sites and additionally for sites over the Baltic Sea and Mediterranean.

Fig. 17. Location of validations sites of AERONET, used for the inter-comparison of AOT retrievals from MERIS L1 data with ground based measurements of AOT.

Fig. 18. Validation of BAER AOT retrievals using MERIS L1 data for the wavelength 0.443 µm against AERONET channel 0.440 µm for collocated data over European and US sites.

53

Fig. 19. Synthetic data retrieval. BAER retrieval results for two different phase functions: experimental LACE-98 and OPAC clean marine, using synthetic test data of Kokhanovsky et al., 2009. The dashed line is the plot of the synthetic test data.

Fig. 20. Instrument degradation according 4. and 5. reprocessing in comparison with the lunar calibration of the SeaWiFS instrument.
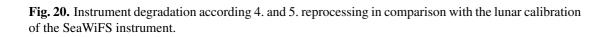
Fig. 21. Global AOT product for 3 May 2006, obtained by BAER, using SeaWiFS GAC data for the generation of monthly averages.

Fig. 22a. Time series of AOT from SeaWiFS channel 1 (0.412 µm) and channel 5 (0.555 µm) for the time span October 1997–May 2008 for the selected regions of interest: BeNeLux-big (Fig. 22a), Po-Valley-big (Fig. 22b), Eastern Europe (Fig. 22c) and Pearl River Delta (Fig. 22d). Linear fits for the trends of the retrieved AOT are presented as dashed lines.

Fig. 22b. Po-Valley-big

58

Fig. 22c. Eastern Europe

59

Fig. 22d. Pearl River Delta